Haverford College

Haverford Scholarship

Faculty Publications

Physics

2016

Evidence for the kinematic Sunyaev-Zel'dovich effect with the Atacama Cosmology Telescope and velocity reconstruction from the Baryon Oscillation Spectroscopic Survey

Emmanuel Schaan

Simone Ferraro

Mariana Vargas-Magana

Bruce Partridge
Haverford College, bpartrid@haverford.edu

Follow this and additional works at: https://scholarship.haverford.edu/physics_facpubs

Repository Citation

Evidence for the kinematic Sunyaev-Zel'dovich effect with the Atacama Cosmology Telescope and velocity reconstruction from the Baryon Oscillation Spectroscopic Survey

Emmanuel Schaan,[1,*] Simone Ferraro,[1,2] Mariana Vargas-Magaña,[3] Kendrick M. Smith,[4] Shirley Ho,[5] Simone Aiola,[6] Nicholas Battaglia,[1] J. Richard Bond,[7] Francesco De Bernardis,[8] Erminia Calabrese,[1,9] Hsiao-Mei Cho,[10] Mark J. Devlin,[11] Joanna Dunkley,[9] Patricio A. Gallardo,[8] Matthew Hasselfield,[1] Shawn Henderson,[8] J. Colin Hill,[12] Adam D. Hincks,[13] Renée Hlozek,[1] Johannes Hubmayr,[14] John P. Hughes,[15] Kent D. Irwin,[16,10] Brian Koopman,[8] Arthur Kosowsky,[6] Dale Li,[10] Thibaut Louis,[9] Marius Lungu,[11] Mathew Madhavacheril,[17] Loïc Maurin,[18] Jeffrey John McMahon,[19] Kavilan Moodley,[20] Sigurd Naess,[9] Federico Nati,[11] Laura Newburgh,[21] Michael D. Niemack,[8] Lyman A. Page,[22] Christine G. Pappas,[22] Bruce Partridge,[23] Benjamin L. Schmitt,[11] Neelima Sehgal,[17] Blake D. Sherwin,[24,2] Jonathan L. Sievers,[25,26] David N. Spergel,[1] Suzanne T. Staggs,[22] Alexander van Engelen,[7] and Edward J. Wollack[27]

(ACTPol Collaboration)

[1]*Department of Astrophysical Sciences, Peyton Hall, Princeton University, Princeton, New Jersey 08544, USA*
[2]*Miller Institute for Basic Research in Science, University of California, Berkeley, California 94720, USA*
[3]*Instituto de Física, Universidad Nacional Autónoma de México, Apartado Postal 20-364, México D.F.04510, México*
[4]*Perimeter Institute for Theoretical Physics, Waterloo, Ontario N2L 2Y5, Canada*
[5]*Department of Physics, Carnegie Mellon University, 5000 Forbes Avenue, Pittsburgh, Pennsylvania 15213, USA*
[6]*Department of Physics and Astronomy, University of Pittsburgh, Pittsburgh, Pennsylvania 15260 USA and Pittsburgh Particle Physics, Astrophysics, and Cosmology Center, University of Pittsburgh, Pittsburgh, Pennsylvania 15260, USA*
[7]*Canadian Institute for Theoretical Astrophysics, University of Toronto, Toronto, Ontario M5S 3H8, Canada*
[8]*Department of Physics, Cornell University, Ithaca, New York 14853, USA*
[9]*Sub-Department of Astrophysics, University of Oxford, Keble Road, Oxford OX1 3RH, United Kingdom*
[10]*SLAC National Accelerator Laboratory, 2575 Sandhill Hill Road, Menlo Park, California 94025, USA*
[11]*Department of Physics and Astronomy, University of Pennsylvania, 209 South 33rd Street, Philadelphia, Pennsylvania 19104, USA*
[12]*Department of Astronomy, Pupin Hall, Columbia University, New York, New York 10027, USA*
[13]*Department of Physics and Astronomy, University of British Columbia (UBC), 6224 Agricultural Road, Vancouver, British Columbia V6T 1Z1, Canada*
[14]*National Institute of Standards and Technology, Boulder, Colorado 80305, USA*
[15]*Department of Physics and Astronomy, Rutgers University, 136 Frelinghuysen Road, Piscataway, New Jersey 08854-8019, USA*
[16]*Department of Physics, Stanford, California 94305, USA*
[17]*Physics and Astronomy Department, Stony Brook University, Stony Brook, New York 11794, USA*
[18]*Instituto de Astrofísica, Pontificía Universidad Católica de Chile, 782-0436 Macul, Santiago, Chile*
[19]*Department of Physics, University of Michigan, Ann Arbor, Michigan 48103, USA*
[20]*Astrophysics and Cosmology Research Unit, School of Mathematics, Statistics and Computer Science, University of KwaZulu-Natal, Durban 4041, South Africa*
[21]*Dunlap Institute, University of Toronto, 50 St. George Street, Toronto, M5S3H4 Ontario, Canada*
[22]*Joseph Henry Laboratories of Physics, Jadwin Hall, Princeton University, Princeton, New Jersey 08544, USA*
[23]*Department of Physics and Astronomy, Haverford College, Haverford, Pennsylvania 19041, USA*
[24]*Berkeley Center for Cosmological Physics, LBL and Department of Physics, University of California, Berkeley, California 94720, USA*
[25]*Astrophysics and Cosmology Research Unit, School of Chemistry and Physics, University of KwaZulu-Natal, Durban 4041, South Africa*
[26]*National Institute for Theoretical Physics (NITheP), University of KwaZulu-Natal, Private Bag X54001, Durban 4000, South Africa*
[27]*NASA/Goddard Space Flight Center, Greenbelt, Maryland 20771, USA*

---

[*]eschaan@astro.princeton.edu

We use microwave temperature maps from two seasons of data from the Atacama Cosmology Telescope at 146 GHz, together with the "Constant Mass" CMASS galaxy sample from the Baryon Oscillation Spectroscopic Survey to measure the kinematic Sunyaev-Zel'dovich (kSZ) effect over the redshift range $z = 0.4$–0.7. We use galaxy positions and the continuity equation to obtain a reconstruction of the line-of-sight velocity field. We stack the microwave temperature at the location of each halo, weighted by the corresponding reconstructed velocity. We vary the size of the aperture photometry filter used, thus probing the free electron profile of these halos from within the virial radius out to three virial radii, on the scales relevant for investigating the missing baryons problem. The resulting best fit kSZ model is preferred over the no-kSZ hypothesis at 3.3 and 2.9σ for two independent velocity reconstruction methods, using 25,537 galaxies over 660 square degrees. The data suggest that the baryon profile is shallower than the dark matter in the inner regions of the halos probed here, potentially due to energy injection from active galactic nucleus or supernovae. Thus, by constraining the gas profile on a wide range of scales, this technique will be useful for understanding the role of feedback in galaxy groups and clusters. The effect of foregrounds that are uncorrelated with the galaxy velocities is expected to be well below our signal, and residual thermal Sunyaev-Zel'dovich contamination is controlled by masking the most massive clusters. Finally, we discuss the systematics involved in converting our measurement of the kSZ amplitude into the mean free electron fraction of the halos in our sample.

I. INTRODUCTION

Measurements of the anisotropy in the cosmic microwave background (CMB) radiation, together with constraints from big bang nucleosynthesis and the Lyman-α forest, tightly constrain the total baryon abundance of the Universe at $z \gtrsim 2$ [1–3]. Reference [4] estimates that at $z = 0$ about 10% of the baryons are found in stars or other neutral medium and that the majority of the rest is thought to be in a warm, diffuse component called the warm-hot intergalactic medium (WHIM). The WHIM has a typical temperature of 10^5–10^7 K and is located in the outskirts of galactic halos where it is too cold and too diffuse to be easily observable with x rays or through the thermal Sunyaev-Zel'dovich (tSZ) effect. The WHIM's cooling time is longer than the Hubble time so that it does not cool to form stars [5]. Due to the difficulty in observing the WHIM using current methods, the spatial distribution and abundance of baryons in the outskirts of galaxies and clusters is still poorly constrained, especially for group-sized or smaller objects. Observations of highly ionized ions in quasar absorption lines provide most of the current observational constraints on its properties (see [6] and references therein). The approach that we describe here complements these measurements by tracing the distribution of free electrons, effectively tracing the overall baryonic distribution around galaxies.

The kinematic Sunyaev-Zel'dovich (kSZ) effect is the shift in CMB photon energy due to Thomson scattering off coherently moving electrons [7,8]. As we discuss below, the kSZ effect depends linearly on the local free electron density n_e, is independent of temperature T_e, and is therefore well suited to probe the low density and low temperature outskirts of galaxies and clusters. This should be contrasted with the x-ray signal ($\propto n_e^2 \sqrt{T_e}$) and the tSZ

signal ($\propto n_e T_e$), which receive their largest contributions from close to the cluster centers. The integrated kSZ signal is proportional to the halo mass, while the integrated tSZ signal scales as a higher power of mass (about $M^{5/3}$). Because of this unique scaling, the kSZ effect becomes larger than the tSZ effect for $M_{200c} \lesssim 2 \times 10^{13}$ (at 146 GHz, for a halo with line-of-sight velocity equal to the one-dimensional rms), making it a useful probe of lower mass galaxy groups, where the missing baryon problem is thought to be more severe. Finally, kSZ measurements probe the electron density profile directly, without spectroscopy or assumptions on the temperature profile. As a result, the kSZ signal is highly complementary with x-ray and tSZ observations. Combining these signals should provide valuable insights on cluster physics.

To lowest order, the kSZ effect is a Doppler shift, and therefore preserves the black body frequency spectrum of the CMB, simply shifting the brightness temperature. In temperature units, the shift $\Delta T^{\text{kSZ}}(\hat{\boldsymbol{n}})$ produced by the kSZ effect is sourced by the free electron *momentum field* $n_e \boldsymbol{v}_e$, and is given by [7,9]

$$\frac{\Delta T^{\text{kSZ}}(\hat{\boldsymbol{n}})}{T_{\text{CMB}}} = -\sigma_T \int \frac{d\chi}{1+z} e^{-\tau(\chi)} n_e(\chi\hat{\boldsymbol{n}},\chi) \frac{\boldsymbol{v}_e}{c} \cdot \hat{\boldsymbol{n}}, \quad (1)$$

where σ_T is the Thomson scattering cross section, $\chi(z)$ is the comoving distance to redshift z, τ is the optical depth to Thomson scattering, n_e and $\boldsymbol{v}_e$ are the *free* electron physical number density and peculiar velocity, and $\hat{\boldsymbol{n}}$ is the line-of-sight direction, defined to point away from the observer. At late times, some fraction of the electrons in galaxies and clusters resides in the neutral medium or in stars and compact objects and does not take part in the Thomson scattering that gives rise to the kSZ effect. We define f_{free} as

the fraction of free electrons compared to the expected cosmological abundance and note that the amplitude of the kSZ signal is directly proportional to it. The precise value of f_{free} is unknown and is expected to depend on redshift and mass; obtaining its value is one of the goals of precision kSZ measurements. For an object with total mass (baryonic plus dark matter) M_{200c}, we expect from Eq. (1) $\Delta T^{kSZ} \approx -0.1\mu K f_{free}(M_{200c}/10^{13}M_\odot)(\boldsymbol{v}_e \cdot \hat{\boldsymbol{n}}/300\,km\,s^{-1})$, where we have taken the typical one-dimensional rms velocity at $z \lesssim 0.5$ to be $300\,km\,s^{-1}$ and have defined M_{200c} to be the mass contained in a spherical volume with mean density 200 times the critical density at the halo redshift.

The kSZ signal is challenging to extract from the CMB, because a given halo can contribute a positive or negative signal with equal probability. The signal nearly cancels in a naïve stacking or cross-correlation analysis. To remedy this, a number of estimators have been proposed [10–16]. The first evidence for the kSZ signal was reported in [17] by using the pairwise velocity method, i.e. the fact that, on average, pairs of galaxies are moving toward rather than away from each other. The Planck team performed a similar analysis in [18] and found evidence for the pairwise signal at 1.8–2.5σ. Here we build upon the work of [11–14,19], noting that if we have independent information on the peculiar velocity, we can weight halos by their velocities and avoid the cancellation. Such estimates for the galaxy velocities can be obtained from the galaxy overdensity field by using the linearized continuity equation as described below.

References [18] and [20] use a similar approach with the Planck data to measure the kSZ signal from halos at redshift $z \simeq 0.1$, traced by a sample of central galaxies from SDSS DR7. They correlated the reconstructed velocity with the measured temperature at separations ranging from 10 to 150 Mpc, finding evidence for the kSZ effect at 3–3.7σ. The large area of the Planck survey allowed one to measure the correlated motion of baryons on large scales and large apertures (5–$18'$).

In this article, we instead focus on the profile of electrons associated with the halos, by correlating the reconstructed velocities with the measured temperature at the same location. We vary the aperture (1–$4.5'$) on physical scales relevant for investigating the "missing baryon" problem and the effect of feedback, from within the virial radius out to three virial radii.

We use CMB data from the Atacama Cosmology Telescope (ACTPol) [21], together with individual velocity estimates for the CMASS catalog of the Baryon Oscillation Spectroscopic Survey (BOSS) DR10 [22] to provide evidence for the kSZ signal with signal to noise ratio $S/N = 3.3$ and 2.9, for the two independent reconstruction methods used.

II. GALAXY SAMPLE

CMASS galaxies have redshifts between 0.4 and 0.7 ($z_{median} = 0.57$) [23]. A high fraction ($\sim 85\%$) of these galaxies resides at the center of galaxy groups or clusters [24] with mean total halo mass of $2 \times 10^{13}M_\odot$ [25–27].

The typical offset between the galaxy position and the halo center of mass is estimated to be $\lesssim 0.2'$ [28], much smaller than the $1.4'$ beam of the temperature map. This makes CMASS galaxies excellent tracers of the center of their host halo.

We use publicly available galaxy stellar mass estimates [29], obtained by fitting a stellar population synthesis model to the observed broadband spectral energy distribution of each CMASS galaxy. These stellar masses range from 10^{11} to $10^{12}M_\odot$, with a mean mass of $2 \times 10^{11}M_\odot$. The individual stellar mass estimates are converted to total masses for the host halos, following [30] (see also [31]). Assuming cosmological baryon abundance (from big bang nucleosynthesis [1] or CMB [2]), we convert each halo mass into baryon mass. We assume that these baryons (hydrogen and helium with primordial abundance [32,33]) are fully ionized, which allows us to convert the baryon mass into the number of free electrons. This yields an estimate for the optical depth to Thomson scattering τ_i of each cluster i. Note that these inferred optical depths are related by a factor of $1/f_{free}$ to the true ones, since part of the electrons are in the neutral medium. This is taken into account consistently in the analysis. A total of 25,537 galaxies overlap with the ACTPol map and are included in the analysis.

III. VELOCITY RECONSTRUCTION

A reconstructed velocity field can be inferred from the observed galaxy number overdensity δ_g by solving the linearized continuity equation in redshift space [34]:

$$\boldsymbol{\nabla} \cdot \boldsymbol{v} + f\boldsymbol{\nabla} \cdot [(\boldsymbol{v} \cdot \hat{\boldsymbol{n}})\hat{\boldsymbol{n}}] = -aHf\frac{\delta_g}{b} \qquad (2)$$

where $f = d\ln\delta/d\ln a$ is the logarithmic linear growth rate. Here we assumed that the galaxy overdensity δ_g is related to the total matter overdensity δ by a linear bias factor b, such that $\delta_g = b\delta$, with b being estimated from the autocorrelation of the galaxy catalog itself.

We use two different implementations of the velocity reconstruction: the first one is used in the BOSS analysis for the purpose of baryon acoustic oscillation peak reconstruction [34,35]. The second one applies a Wiener filter to the galaxy number density field [36]. We refer to the two methods as VR1 and VR2 respectively. Both implementations are tested on BOSS mock catalogs with realistic mask and selection function by comparing the "true" and reconstructed velocities. Using the PTHalos DR11 mock catalogs [37], we find a correlation coefficient between true and reconstructed velocities of $r \simeq 0.65$ and 0.67, and a multiplicative bias $\sigma_{v_{rec}}/\sigma_{v_{true}}$ of 0.64 and 0.69 for VR1 and VR2 respectively. The two methods are compared in detail in an upcoming paper [36].

IV. MICROWAVE TEMPERATURE MAPS

We use a map of the microwave intensity at 146 GHz from ACTPol, a polarization sensitive receiver on the six meter Atacama Cosmology Telescope in Chile. Our map covers approximately 13° in declination around the celestial equator, from right ascension −10 to 40°, and combines observations from ACT season 3 and 4 (2009 and 2010 data) [38] and ACTPol season 1 and 2 (2013 and 2014 data) [21]. The effective beam full width at half maximum (FWHM) is 1.4′, and the map noise level is approximately $14\mu K \cdot \text{arcmin}$, although it varies from 10 to $16\mu K \cdot \text{arcmin}$ across the map.

An aperture photometry (AP) filter is applied at the position of each galaxy, and yields a noisy estimate δT_i of the kSZ signal from the host halo. Applying the AP filter consists in averaging the value of the pixels within a disk of radius θ_{disk}, and subtracting the average of the pixels in an adjacent, equal area ring with external radius $\theta_{\text{ring}} = \sqrt{2}\theta_{\text{disk}}$. This estimate is dominated by primary CMB fluctuations (for aperture radii larger than 2′) and map noise (for aperture radii smaller than 2′), and is also affected by tSZ, galactic emission and other foregrounds. However, all these contaminants are uncorrelated with the cluster line-of-sight velocity and are expected to average out once weighted by the reconstructed velocities that have alternating sign. If the electron density profile were known, an optimal linear filter could be applied [12–16]. Due to the large uncertainty in the profile, the matched filter can be highly biased if the assumed profile is incorrect [39], so we prefer the aperture photometry filter in this analysis.

V. ANALYSIS

For each object in our sample, we define its Thomson optical depth estimate as τ_i and its reconstructed velocity projected in the line-of-sight, $\hat{n}$ direction, as $v_{\text{rec},i}$. We define a number α as the best fit slope in the relation between the expected signal $\tau_i v_{\text{rec},i}$ and the measured kSZ signal,

$$\frac{\delta T_i}{T_{\text{CMB}}} = -\alpha \tau_i \frac{v_{\text{rec},i}}{c}. \tag{3}$$

Finding α consistent with zero means no detection of the kSZ effect, while finding α of order unity when the filter size is large enough to encompass the whole cluster corresponds to a number of free electrons consistent with the cosmological abundance. While α is directly proportional to the fraction of free electrons f_{free} within the filter, the proportionality coefficient is a nontrivial function of several variables (such as the filter size and shape, the baryon profile, the uncertainties in mass and velocity etc.). Accounting for these effects is required in order to constrain f_{free} from our measurement, but is not necessary for the purpose of detection.

For each aperture size θ_{disk}, the best fit value of α is obtained by minimizing

$$\sum_i \frac{(\delta T_i/T_{\text{CMB}} + \alpha \tau_i v_{\text{rec},i}/c)^2}{\sigma_i^2}, \tag{4}$$

where the sum runs over all objects in our sample, and σ_i^2 is the variance of the filter output δT_i caused by primary CMB fluctuations and noise.[1] The inverse-variance weighting $\propto 1/\sigma_i^2$ emphasizes the halos that fall on less noisy parts of the CMB map. The temperature map is split into three patches with roughly uniform exposure time and noise level. We estimate σ_i on each patch as the standard deviation of the aperture photometry temperatures measured on that patch. Minimizing Eq. (4) yields the best fit α,

$$\alpha = -\frac{\sum_i (\delta T_i/T_{\text{CMB}})(\tau_i v_{\text{rec},i}/c)/\sigma_i^2}{\sum_i (\tau_i v_{\text{rec},i}/c)^2/\sigma_i^2}. \tag{5}$$

We repeat this analysis for various aperture radii. The best fit coefficient α is shown as a function of AP filter radius θ_{disk} in Fig. 1. The various measurements of α for different θ_{disk} are correlated since the data for a smaller θ_{disk} is a subset of the data for a larger θ_{disk}. In order to estimate the covariance matrix between the α for the various θ_{disk}, we repeat the analysis above on 500 mock CMB maps, which include inhomogeneous noise due to the spatially varying depth of observation, as well as the observed power spectrum of foregrounds. This method has the advantage of preserving the correlations in position and velocity for the BOSS objects, as well as the residual CMB correlations and the occasional overlap between the AP filters. The covariance matrix is shown in the bottom panel of Fig. 2.

The CMASS halos have a typical angular size of $\theta_{\text{vir}} = 1.4′$, while the ACTPol beam is $\sigma_{\text{beam}} = 0.6′$ (corresponding to a FWHM of 1.4′). Given the measurement uncertainties, it is reasonable to approximate the projected electron profile by a Gaussian of standard deviation $\sqrt{\theta_{\text{vir}}^2 + \sigma_{\text{beam}}^2} = 1.5′$. From this Gaussian profile, we predict the template for α as a function of θ_{disk}, by applying the corresponding AP filters to the Gaussian profile. Intuitively, for small θ_{disk}, the cluster kSZ signal contributes to the disk and the ring of the AP filter, which leads to a cancellation. For large θ_{disk}, the cluster signal is entirely included in the disk of the AP filter, and the template goes to unity. The dashed lines in Fig. 1 correspond to this template, after fitting for an overall multiplicative amplitude. We quantify the statistical significance (preference of the kSZ model over the "no kSZ hypothesis") as

---

[1]Here noise is taken to include not only detector noise, but all other effects that are uncorrelated with the signal, such as fluctuations in the atmosphere, and galactic and extragalactic foregrounds.
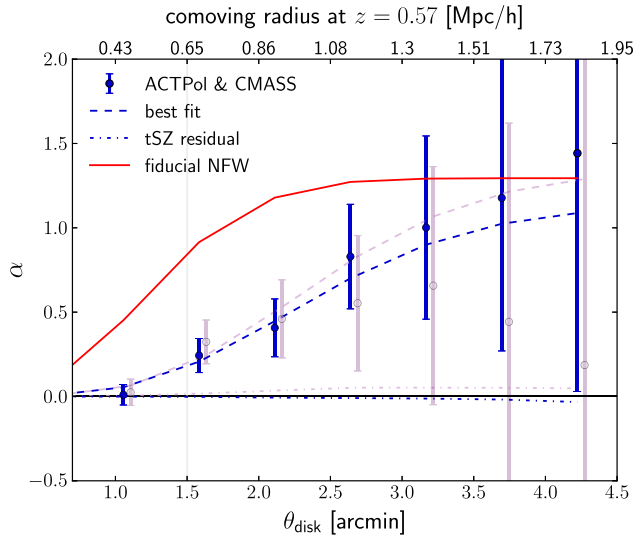
FIG. 1.   Measured coefficient α (points with error bars) as a function of the angular radius θ_{disk} of the AP filter. We have defined α in Eq. (5) as the ratio of the temperature fluctuation to the expected signal if the aperture contained all of the baryons associated with the halo. The rate of change of α with θ_{disk} is a proxy for the average baryon profile of our sample. For large apertures where baryons are thought to trace the dark matter, we expect α to approach 1. The best fit curve (dashed line) is obtained by assuming a Gaussian projected profile with a scale of 1.5′ (sum in quadrature of the beam and the typical virial radius). The tSZ residual (dot-dashed line) is negligible after masking the 1126–2881 clusters more massive than $10^{14} M_{\odot}$. The blue points and curves correspond to the velocity reconstruction method VR1, while the purple ones correspond to VR2. The kSZ signal is measured with $S/N = \sqrt{\Delta\chi^2} = 3.3$ for VR1 and 2.9 for VR2. The vertical gray line shows the position of the typical virial radius. The red line shows the expected signal for a projected NFW profile convolved with the beam. If the baryons followed the dark matter, then this NFW curve would be a good fit to the data.
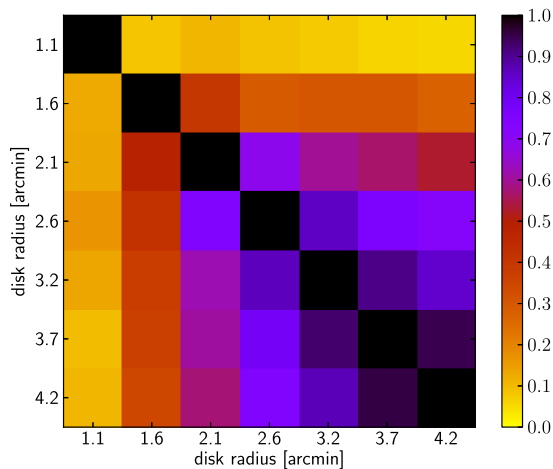
FIG. 2.   Correlation coefficient matrix for the different aperture radii, for VR1 (above the diagonal) and VR2 (below the diagonal). The data points in Fig. 1 are highly correlated, especially for the largest apertures. The signal to noise ratio is dominated by the three smallest apertures.

$S/N = \sqrt{\Delta\chi^2} = \sqrt{\chi^2_{null} - \chi^2_{bf}}$, where χ^2_{null} and χ^2_{bf} refer to the χ^2 statistics applied to the null hypothesis and the best fit respectively. These were computed using the full covariance matrix, accounting for the correlation between the different apertures. We checked that numerical convergence errors on the covariance matrix affect the $\sqrt{\Delta\chi^2}$ value by less than 5%. This signal to noise ratio is the inverse of the relative uncertainty on the best fit amplitude. We measure the kSZ signal with $S/N = 3.3$ for VR1 and 2.9 for VR2, with consistent amplitudes. For comparison, the red line in Fig. 1 shows the expected signal assuming that the gas is fully ionized and traces the dark matter perfectly. We assumed an Navarro-Frenk-White (NFW) profile truncated at $1.5 R_{vir}$,[2] which we projected along the line of sight, convolved with the beam, and to which we applied the aperture photometry filters.

VI. NULL TESTS AND SYSTEMATICS

A number of null tests are performed, as shown in Fig. 3. The procedure described to estimate the covariance matrix provides a first null test. It shows that the kSZ signal is only detected when analyzing the true temperature map, which means that the signal is not due to unexpected features of the galaxy catalog. We further confirm that the kSZ signal is only detected when the correct velocity is attributed to each object, by shuffling the velocities $v_{rec,i}$ among the clusters in our sample. In all cases, the kSZ signal disappears and the result becomes consistent with the null hypothesis.

As explained above, the tSZ signal is typically larger than the kSZ signal for massive clusters ($M_{200c} \gtrsim 2 \times 10^{13} M_{\odot}$ at 146 GHz, for a halo with line-of-sight velocity equal to the one-dimensional rms). Because the tSZ signal is uncorrelated with the line-of-sight velocity and is weighted by alternate signs [see Eq. (5)], its contamination to α is mitigated. We estimate the size of the tSZ contamination to the value of α by replacing the measured cluster temperatures δT_i by estimates for their tSZ signal [31,40] based on their stellar masses. We find the tSZ contamination to be important when including clusters with total mass greater than a few $\times 10^{14} M_{\odot}$. Indeed, these objects are rare enough that the cancellation in the numerator of Eq. (5) is incomplete. Masking objects with $M_{200} > 10^{14} M_{\odot}$, together with a 1′ region around them, is sufficient to limit the tSZ contamination to less than 10% of the statistical uncertainty on α. This removes 1126 objects (for the smallest AP size) to 2881 objects (for the largest AP size) from the analysis.

We assess the amplitude of extragalactic thermal dust contamination from these halos by stacking the CMB map (with uniform weight) at the object positions. This

---

[2]We have checked that the result within R_{vir} is very much independent of the truncation radius.
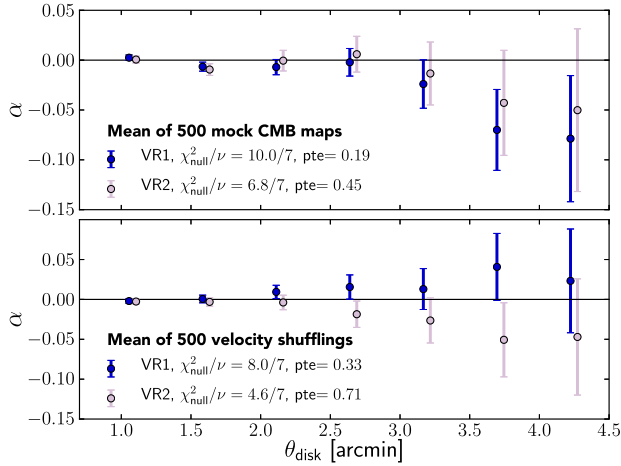
FIG. 3.   Top panel: Mean of 500 null tests obtained by replacing the ACTPol map by a mock CMB map. Bottom panel: Mean of 500 null tests obtained by shuffling the reconstructed velocities among the CMASS objects. Both panels show that the kSZ signal is only detected when analyzing the true ACTPol map and when assigning the correct velocity to each cluster.

measures the sum of the dust emission and tSZ contamination. For the lower mass halos, the signal is consistent with zero, and will therefore be negligible when weighting by alternating sign velocities. For the more massive halos, we measure an overall decrement, meaning that dust emission is subdominant to tSZ, which we control by masking the most massive halos. Therefore dust emission is not expected to be a significant contaminant.[3]

Our analysis pipeline is tested on realistic mock kSZ realizations: a kSZ template is obtained by populating BOSS mock catalogs (PTHalos DR11 [37]) of galaxy positions and velocities with Gaussian cluster profiles and then added to the CMB map, which provides the correct noise level. These mock maps are then analyzed the same way as the real data, by using both the real and reconstructed velocities, obtaining consistent results. The loss in signal to noise when using the reconstructed rather than the real velocities is equal to the correlation coefficient r as expected. We estimate the effect of cluster miscentering by adding an offset of $0.2'$ (which is roughly the expected rms miscentering [28]) to the cluster centers in the mocks. This leads to less than 3% change in α.

VII. INTERPRETATION

We have presented evidence for the kSZ signal with overall $S/N \simeq 3$. We defined a coefficient α as the best fit

---

[3]Galactic dust and the bulk of the cosmic infrared background emission are uncorrelated with the CMASS galaxy positions and therefore are only an additional source of noise, which is included in the covariance matrix. The Doppler boosted dust emission from these galaxies is correlated with the line-of-sight velocities, and we estimate it to be smaller than the kSZ signal by a factor 10–100.

proportionality constant between the AP filter output and the expected kSZ signal. This number α can only be interpreted as the free electron fraction f_{free} if all of the electrons associated with each cluster are within the filter aperture, if there is no effect from galaxy overlap, if all the galaxies in our sample are central galaxies and if both the velocities and masses are known exactly. This is clearly not the case here, so the physical interpretation of α is not straightforward. We now briefly discuss these effects, which determine the relationship between α and f_{free}, and defer a careful and in-depth analysis of these effects to upcoming work.

If the kSZ emission from the object does not entirely fall within the inner disk of the AP filter, part of the signal will be subtracted off, reducing the observed value of α. This is clearly visible in Fig. 1, for small θ_{disk}: the size of the disk for $\theta_{\text{disk}} \ll 2'$ is smaller than the extent of the emission and the signal is canceled by the surrounding ring. For large apertures θ_{disk}, we expect this cancellation to disappear and α to asymptote to f_{free}.

The gas spatial profile would then determine the rate of increase of α from 0 to f_{free}. In fact, Fig. 1 can be thought of as a proxy for the average baryon profile of our sample. However, the noise from primary CMB fluctuations also increases with θ_{disk}, making it difficult to disentangle the free electron fraction f_{free} from the spatial size of the cluster.

As an illustration, Fig. 1 compares our measurements with the expected signal if the electron profile followed exactly the dark matter profile (red line). Within the virial radius, the data suggest that the electron profile is less steep than the dark matter profile, and only includes a fraction of the cosmological abundance of baryons. This is new evidence for the missing baryon problem [4], independent of astrophysical assumptions, and could hint at the presence of feedback, pushing the gas to the outskirts of the halo. While we assumed $f_{\text{free}} = 1$ for the expected signal, the qualitative conclusion of a shallower observed profile still holds for any reasonable value of f_{free}. Further away from the center ($>2R_{\text{vir}}$), our data are consistent with the full cosmological abundance; however our statistical power is limited by the small number of overlapping CMASS halos. As the area of high resolution CMB maps increases, this method will eventually place strong constraints on the baryon abundance in the outskirts of galaxies and clusters.

The reconstructed velocities are biased low and are not 100% correlated with the true velocities. Therefore, α differs from f_{free} by an additional factor of $r\sigma_{v_{\text{true}}}/\sigma_{v_{\text{rec}}}$ (1.02 for VR1 and 0.97 for VR2), as can be inferred from Eq. (5).

We use an average stellar mass to halo mass relation. The typical intrinsic scatter in this relation [30,31], as well as potential errors on the stellar mass determination, can lead to a bias in α of up to $\sim 40\%$.

The presence of extra free electrons with correlated velocities (unbound or associated with a different cluster)

within a single aperture is expected to bias α high. This effect can be interpreted as a two-halo term in the kSZ correlation function, where the presence of additional mass correlated with the galaxies used for stacking contributes a signal at large enough separations.

VIII. OUTLOOK

As the overlap between large-scale structure data sets and high sensitivity CMB maps increases, the significance of kSZ detections will see a rapid improvement. Future surveys such as Advanced ACTPol [41] and SPT-3G [42] should enable a few percent-level precision kSZ measurement.

Combined with a better understanding of the relationship between the observed signal and the underlying physical properties of the sample, these high-significance detections will enable a precise measurement of the free electron fraction and the baryon profile of the low-density regions in the outskirts of galaxies and clusters, which are sensitive to the feedback mechanisms at play and are believed to host the majority of the gas.

These measurements can be performed as a function of mass and redshift, and combined with tSZ and x-ray observations of the same objects to independently measure density and temperature profiles. These measurements will shed new light on galaxy evolution and feedback processes within clusters, which can be used to improve the cosmological constraints from cluster counts [43,44] and our understanding of the matter power spectrum on small scales [45,46].

Once the astrophysical quantities are well characterized, the kSZ signal itself can also be used for a number of cosmological applications, such as constraining bulk flows [47,48], probing neutrino physics [49] and testing general relativity [50,51].

[1] R. J. Cooke, M. Pettini, R. A. Jorgenson, M. T. Murphy, and C. C. Steidel, Astrophys. J. **781**, 31 (2014).

[2] P. A. R. Ade, N. Aghanim *et al.* (Planck Collaboration), arXiv:1502.01589.

[3] G. Hinshaw, D. Larson, E. Komatsu *et al.*, Astrophys. J. Suppl. Ser. **208**, 19 (2013).

[4] M. Fukugita and P. J. E. Peebles, Astrophys. J. **616**, 643 (2004).

[5] R. Cen and J. P. Ostriker, Astrophys. J. **650**, 560 (2006).

[6] M. Bonamente, J. Nevalainen, E. Tilton *et al.*, Mon. Not. R. Astron. Soc. **457**, 4236 (2016).

[7] R. A. Sunyaev and Ya. B. Zel'dovich, Comments Astrophys. Space Phys. **4**, 173 (1972).

[8] R. A. Sunyaev and Ya. B. Zel'dovich, Mon. Not. R. Astron. Soc. **190**, 413 (1980).

[9] J. P. Ostriker and E. T. Vishniac, Astrophys. J. **306**, L51 (1986).

[10] O. Doré, J. F. Hennawi, and D. N. Spergel, Astrophys. J. **606**, 46 (2004).

[11] A. Stebbins, New Astron. Rev. **50**, 918 (2006).

[12] S. Ho, S. Dedeo, and D. Spergel, arXiv:0903.2845 [Phys. Rev. D (to be published)].

[13] J. Shao, P. Zhang, W. Lin, Y. Jing, and J. Pan, Mon. Not. R. Astron. Soc. **413**, 628 (2011).

[14] M. Li, R. E. Angulo, S. D. M. White, and J. Jasche, Mon. Not. R. Astron. Soc. **443**, 2311 (2014).

[15] P. G. Ferreira, R. Juszkiewicz, H. A. Feldman, M. Davis, and A. H. Jaffe, Astrophys. J. **515**, L1 (1999).

[16] S. Bhattacharya and A. Kosowsky, Phys. Rev. D **77**, 083004 (2008).

[17] N. Hand, G. E. Addison, E. Aubourg *et al.*, Phys. Rev. Lett. **109**, 041101 (2012).

[18] P. A. R. Ade, N. Aghanim *et al.* (Planck Collaboration), Astron. Astrophys. **586**, A140 (2016).

[19] G. Lavaux, N. Afshordi, and M. J. Hudson, Mon. Not. R. Astron. Soc. **430**, 1617 (2013).

[20] C. Hernández-Monteagudo, Y.-Z. Ma, F. S. Kitaura *et al.*, Phys. Rev. Lett. **115**, 191301 (2015).

[21] S. Naess, M. Hasselfield, J. McMahon *et al.*, J. Cosmol. Astropart. Phys. 10 (2014) 007.

[22] C. P. Ahn, R. Alexandroff, C. Allende Prieto *et al.*, Astrophys. J. Suppl. Ser. **211**, 17 (2014).

[23] L. Anderson, É. Aubourg, S. Bailey *et al.*, Mon. Not. R. Astron. Soc. **441**, 24 (2014).

[24] S. E. Nuza, A. G. Sánchez, F. Prada *et al.*, Mon. Not. R. Astron. Soc. **432**, 743 (2013).

[25] H. Miyatake, S. More, R. Mandelbaum, M. Takada, D. N. Spergel, J.-P. Kneib, D. P. Schneider, J. Brinkmann, and J. R. Brownstein, Astrophys. J. **806**, 1 (2015).

[26] S. More, H. Miyatake, R. Mandelbaum, M. Takada, D. N. Spergel, J. R. Brownstein, and D. P. Schneider, Astrophys. J. **806**, 2 (2015).

[27] M. Madhavacheril, N. Sehgal, R. Allison *et al.*, Phys. Rev. Lett. **114**, 151302 (2015).

[28] M. R. George, A. Leauthaud, K. Bundy, A. Finoguenov, C.-P. Ma, E. S. Rykoff, J. L. Tinker, R. H. Wechsler, R. Massey, and S. Mei, Astrophys. J. **757**, 2 (2012).

[29] C. Maraston, J. Pforr, B. M. Henriques *et al.*, Mon. Not. R. Astron. Soc. **435**, 2764 (2013).

[30] A. Kravtsov, A. Vikhlinin, and A. Meshscheryakov, arXiv:1401.7329 [Astrophys. J. (to be published)].

[31] P. A. R. Ade, N. Aghanim *et al.* (Planck Collaboration), Astron. Astrophys. **557**, A52 (2013).

[32] E. Aver, K. A. Olive, R. L. Porter, and E. D. Skillman, J. Cosmol. Astropart. Phys. 11 (2013) 017.

[33] Y. I. Izotov, G. Stasińska, and N. G. Guseva, Astron. Astrophys. **558**, A57 (2013).

[34] N. Padmanabhan, X. Xu, D. J. Eisenstein, R. Scalzo, A. J. Cuesta, K. T. Mehta, and E. Kazin, Mon. Not. R. Astron. Soc. **427**, 2132 (2012).

[35] M. Vargas-Magaña *et al.*, arXiv:1509.06384.

[36] K. M. Smith *et al.* (to be published).

[37] M. Manera, R. Scoccimarro, W. J. Percival *et al.*, Mon. Not. R. Astron. Soc. **428**, 1036 (2013).

[38] S. Das, T. Louis, M. R. Nolta *et al.*, J. Cosmol. Astropart. Phys. 4 (2014) 014.

[39] S. Ferraro and B. Hensley, Mon. Not. R. Astron. Soc. **451**, 1606 (2015).

[40] J. P. Greco, J. C. Hill, D. N. Spergel, and N. Battaglia, Astrophys. J. **808**, 151 (2015).

[41] S. W. Henderson, R. Allison, J. Austermann *et al.*, arXiv:1510.02809 [J. Low Temp. Phys. (to be published)].

[42] B. A. Benson, P. A. R. Ade, Z. Ahmed *et al.*, Proc. SPIE Int. Soc. Opt. Eng. **9153**, 91531P (2014).

[43] P. A. R. Ade, N. Aghanim *et al.* (Planck Collaboration), arXiv:1502.01597.

[44] M. Hasselfield, M. Hilton, T. A. Marriage *et al.*, J. Cosmol. Astropart. Phys. 7 (2013) 008.

[45] D. H. Rudd, A. R. Zentner, and A. V. Kravtsov, Astrophys. J. **672**, 19 (2008).

[46] K. Osato, M. Shirasaki, and N. Yoshida, Astrophys. J. **806**, 186 (2015).

[47] K. Mody and A. Hajian, Astrophys. J. **758**, 4 (2012).

[48] P. A. R. Ade, N. Aghanim *et al.* (Planck Collaboration), Astron. Astrophys. **561**, A97 (2014).

[49] E.-M. Mueller, F. de Bernardis, R. Bean, and M. D. Niemack, Phys. Rev. D **92**, 063501 (2015).

[50] A. Kosowsky and S. Bhattacharya, Phys. Rev. D **80**, 062003 (2009).

[51] E.-M. Mueller, F. de Bernardis, R. Bean, and M. Niemack, Astrophys. J. **808**, 47 (2015).